



## OPEN ACCESS

## EDITED BY

Wen Nie,  
Jiangxi University of Science and  
Technology, China

## REVIEWED BY

Qibin Lin,  
University of South China, China  
Xiaoran Wang,  
China University of Mining and  
Technology, China

Peng Li,  
University of Science and Technology  
Beijing, China

## \*CORRESPONDENCE

Ruide Lei,  
✉ leiruide123@163.com

RECEIVED 28 August 2024

ACCEPTED 14 October 2024

PUBLISHED 01 November 2024

## CITATION

Liu G, Lei R, Huang L, Li M and Zhou J (2024)  
Study on the mining response law and coal  
burst risk assessment of an isolated working  
face.  
*Front. Earth Sci.* 12:1487505.  
doi: 10.3389/feart.2024.1487505

## COPYRIGHT

© 2024 Liu, Lei, Huang, Li and Zhou. This is an  
open-access article distributed under the  
terms of the [Creative Commons Attribution  
License \(CC BY\)](https://creativecommons.org/licenses/by/4.0/). The use, distribution or  
reproduction in other forums is permitted,  
provided the original author(s) and the  
copyright owner(s) are credited and that the  
original publication in this journal is cited, in  
accordance with accepted academic practice.  
No use, distribution or reproduction is  
permitted which does not comply with  
these terms.

# Study on the mining response law and coal burst risk assessment of an isolated working face

Guojun Liu<sup>1,2</sup>, Ruide Lei<sup>3,4,5\*</sup>, Ling Huang<sup>3</sup>, Menglai Li<sup>4</sup> and Jiankun Zhou<sup>4</sup>

<sup>1</sup>Hunan Engineering Research Center of Development and Application of Ceramsite Concrete Technology, Hunan City University, Yiyang, China, <sup>2</sup>Key Laboratory of Green Building and Intelligent Construction in Higher Educational Institutions of Hunan Province, Hunan City University, Yiyang, China, <sup>3</sup>College of Civil Engineering, Sichuan University of Science and Engineering, Zigong, China, <sup>4</sup>Key Laboratory of Shale Gas Exploration, Ministry of Natural Resources, Chongqing Institute of Geology and Mineral Resources, Yubei, China, <sup>5</sup>Key Laboratory of Safety and High-Efficiency Coal Mining, Ministry of Education, Anhui University of Science and Technology, Huainan, China

With the increasing demand for coal resources and the unreasonable arrangement of subsequent working faces, mining activities in isolated working faces are more likely to induce coal burst accidents. In this study, the minimum distance principle is utilized as the risk assessment indicator and the quantitative theory is introduced to evaluate coal burst risk in isolated working faces. Through a case study in 1,304 isolated working face of Yangcheng Coal Mine, the key factors affecting the risk of coal burst were identified, and a three-dimensional coal burst risk assessment model was constructed to evaluate the risk of the isolated working face. The results show that as the working face advances, the abutment pressure and elastic strain energy density in front of the working face increase to the peak value in a positive exponential relationship at first and then decrease to *in situ* stress, which presents an upward convex trend. Under different excavation steps, the concentration coefficient of the peak stress gradually increases. The influence range of the abutment pressure of the working face gradually increases. Compared with one-dimensional and two-dimensional evaluation functions, the three-dimensional function significantly improves the accuracy of risk assessment and successfully identifies strong coal and gas outburst risks. Additionally, the model not only enhances the precision of risk assessment but also quantifies the assessment parameters.

## KEYWORDS

coal burst, risk evaluation, isolated working face, quantitative theory, elastic strain energy density

## 1 Introduction

Coal burst is a typical dynamic disaster often accompanied by the sudden ejection of coal during underground mining activities (Zhao et al., 2018a; Wen et al., 2019; Tai et al., 2022; Wang P. et al., 2024). In recent years, there has been a significant expansion of coal mining operations, with corresponding increases in mining depths. As the mining depths increase, the engineering conditions encountered in mining activities become

more complex, particularly the issue of high *in situ* stress due to mining depth, faults, and tectonic areas with isolated working faces (Guo et al., 2017; Zhao et al., 2018b; Li et al., 2022; Wang et al., 2024a; Wang et al., 2024b). Under the action of high stress accumulation and complex tectonic stress, the instability of island working faces is more likely to occur. The reason for this is the substantial accumulation of elastic energy, which can potentially lead to significant geotechnical hazards such as mine earthquakes or severe coal burst accidents (Xie et al., 2015; Pan et al., 2018; Li et al., 2021; Li et al., 2024). The instability of isolated working faces poses a severe threat to the safety of coal mining operations and has been responsible for numerous casualties. Therefore, it is imperative to develop effective methods for risk assessment and dynamic failure prediction.

Coal burst risk evaluation methods can be categorized into the following: qualitative evaluation method and quantitative evaluation method. The qualitative method assesses the risk of coal burst by summarizing the characteristics of the coal burst phenomenon. Based on the characteristics of mine micro-seismic data, Cao et al. (2022) proposed a neural network for coal burst prediction that is driven by the fusion of data and knowledge. Zhou J. et al. (2022) investigated the coal burst mechanism of isolated working surfaces and established a numerical model to describe the evolution of static and dynamic stress. The mechanism of coal burst disasters is highly complex, involving numerous influencing factors throughout the disaster's preparation and development process. For instance, island mining on a coal face can lead to high stress accumulation before catastrophic failure, which may then trigger a coal burst. These prediction models struggle to quantify the relationships between control factors and the timing and location of coal burst accidents, which hampers the ability to accurately and scientifically evaluate the risk of coal bursting (Guo et al., 2019; Xu et al., 2019; Cao et al., 2023). However, the aforementioned evaluation methods primarily offer a qualitative assessment of prevention measures prior to coal mining, rather than providing a quantitative analysis.

To improve the accuracy of coal burst evaluations, quantitative evaluation methods are introduced to study the coal burst grade evaluation model for isolated working faces. The quantitative evaluation methods mainly include the comprehensive index method (Ahmad et al., 2021), possibility index diagnosis method (Zhou K. Y. et al., 2022), and fuzzy mathematics method (Tang et al., 2010). The comprehensive index method describes the relationship between coal burst risk and various mining conditions. Wu et al. (2019) optimized the least square support vector machine (LSSVM) method through the particle swarm optimization algorithm and proposed a new probability model for tunnel coal burst prediction using Copula's theory. Dou et al. (2018) analyzed the multi-dimensional information of micro-seismic data during the mining process, conducted early warning of coal burst events through comprehensive analysis, and established a multi-parameter index normalization system for the early warning of micro-seismic coal burst. Di et al. (2023) proposed a comprehensive early-warning mode based on a deep learning algorithm through the comprehensive analysis of micro-seismic, acoustic emission and electromagnetic radiation signals. Wang et al. (2015) established a multi-index model for predicting coal mine rock burst by combining fuzzy matter theory, information entropy theory, and proximity theory. He et al. (2017) performed a comprehensive analysis of

stress distribution and dynamic stress perturbations based on stress monitoring. Using Bayesian networks, Wang et al. (2022) quantified the probabilistic relationship between rock burst and its different types, and predicted the occurrence probability of rock burst by integrating multiple indicators. Moreover, Du et al. (2021) adopted the Bayesian method and combined the traditional comprehensive index method with the likelihood index diagnosis method to build a comprehensive risk assessment. Liu et al. (2023) established a multi-layer fuzzy comprehensive evaluation model based on the analytic hierarchy process–fuzzy comprehensive evaluation (AHP-FCE) method. Several influencing factors of rock burst risk were determined, and the evaluation model was calculated using a second-order fuzzy mathematical calculation method. It was found that the evaluation results are consistent with those of the comprehensive index method and the possibility index method. Dong et al. (2013) conducted a study on the AHP applied to the coal mine safety evaluation. Sun et al. (2009) combined fuzzy mathematics and neural networks to propose a fuzzy neural network prediction model for rock burst risk. These quantitative evaluation methods contribute to a more precise and data-driven approach to assessing coal burst risk, which is essential for the effective management and prevention of coal burst incidents in mining operations. The quantitative evaluation method is a significant branch of multivariate analysis methods and serves as an effective tool for processing quantitative data (He et al., 2023; Hao and Niu, 2014; Hu et al., 2014; Wang et al., 2012). This approach allows for the development of more effective strategies to mitigate the risks and enhance the safety of coal mining operations. Furthermore, quantitative theory evaluation and forecasting methods can overcome the limitations of scoring or indexing methods, providing a more robust framework for assessing and managing the risks associated with coal burst disasters. The traditional quantitative model has made some progress in evaluating the risk of rock burst, but there are still areas for improvement. For example, the comprehensive index method captures the relationship among risk factors from a holistic perspective, but its weight allocation relies on expert judgment and is susceptible to subjective influence. The fuzzy mathematical method has an advantage in predicting uncertainty, but it is limited by the complexity of establishing fuzzy sets and defining membership functions. The possibility index diagnostic method is effective in rapidly identifying high-risk areas, but it still lacks in providing complex multivariate analysis. Quantitative theoretical evaluation and prediction techniques are used in this study not only because of their competence in data analysis but also because of their ability to overcome the shortcomings of scoring or indexing methods.

Drawing on the aforementioned research, this study performs a comprehensive examination of coal outburst risk assessment for isolated mining faces, grounded in quantitative theory and the principle of minimum distance. Through the detailed analysis of geological and engineering parameters that influence coal outburst risk, a three-dimensional evaluation model is developed. The utility of various assessment methodologies is further evaluated by integrating numerical simulations with case studies for comparative analysis. This paper is organized as follows: Sections 2, 3 present a numerical simulation analysis on the abutment pressure and elastic strain energy during the mining process; Section 4 establishes a coal burst grade evaluation model for isolated working faces based on



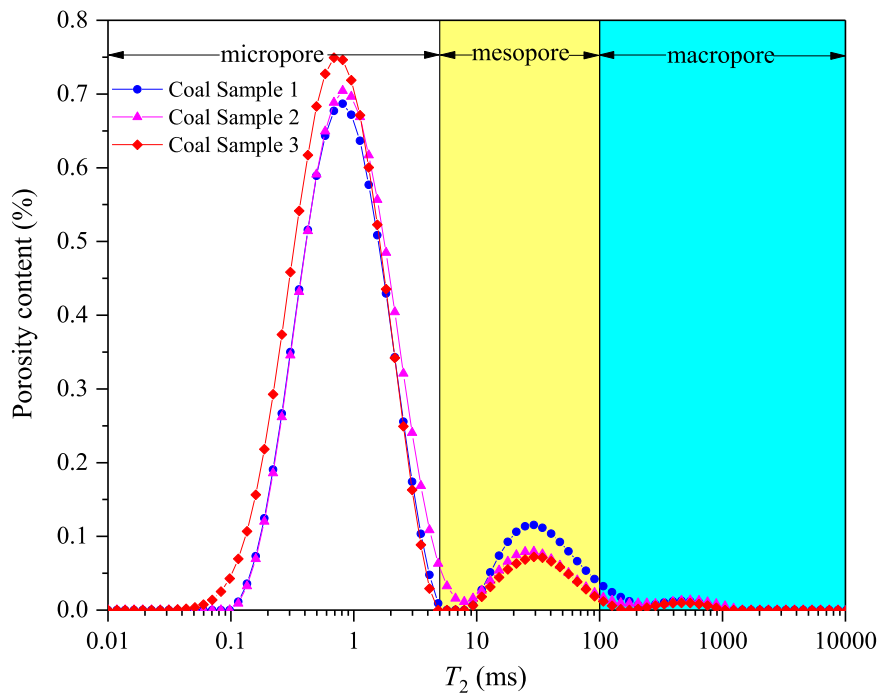


FIGURE 2  
T<sub>2</sub> distribution of typical coal samples.

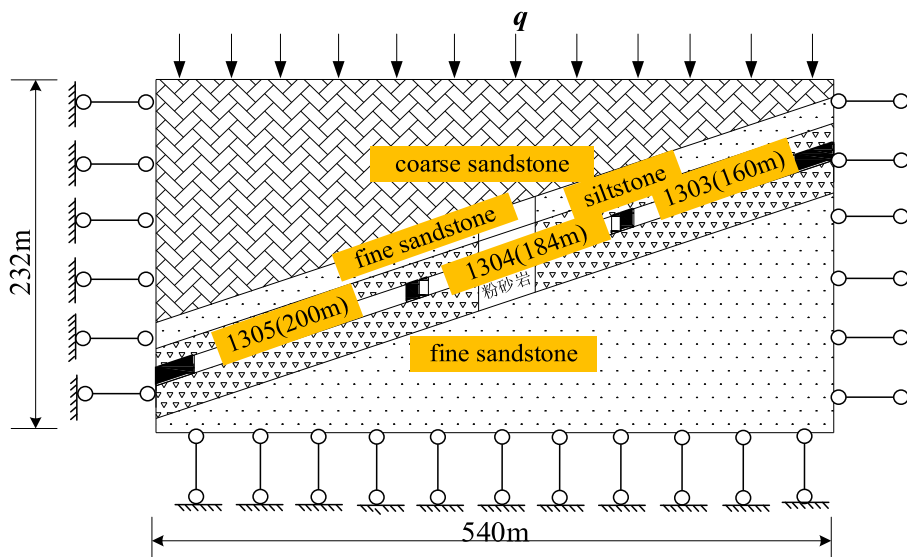


FIGURE 3  
Model geometry.

### 2.3 Physical and mechanical parameters

The mechanical parameters of the coal-rock mass layer in the model are determined according to the actual rock mechanical properties of the Yangcheng Mine, as listed in Table 1. It should be noted that  $E_b$  represents the bulk modulus,  $\rho$  represents the density,  $T$  represents the thickness,  $E_s$  represents the shear modulus,

$c$  represents the cohesion,  $\sigma_t$  represents the tensile strength, and  $\phi$  represents the internal friction angle.

According to the mechanical characteristics of the coal-rock mass, the coal-rock mass will be damaged in different forms when the load borne by the coal-rock mass is greater than its ultimate strength and will maintain a certain residual strength after plastic deformation and failure. Therefore, the Mohr–Coulomb criterion is

TABLE 1 Physical and mechanical parameters of coal-rock mass.

Rock stratum	Lithology	$T$ (m)	$\rho$ (kg/m <sup>3</sup> )	$E_b$ (GPa)	$E_s$ (GPa)	$c$ (MPa)	$\sigma_t$ (MPa)	$\varphi$ (°)
Roof	Coarse sandstone	10	2,500	24	14	10.3	8.9	37
	Medium-fine sandstone	14	2,600	20	11	8.3	4.9	37
	Siltstone	10	2,630	15.6	10.8	7.2	5.0	44
Coal seam	3# Coal	7.5	1,370	2.9	1.65	3.5	1.9	30
Floor	Siltstone	4	2,500	15.6	10.8	7.2	5.0	44
	Fine sandstone	14	2,570	23	12	7.5	2.2	32

utilized in this study. The modified Mohr–Coulomb model strength criterion is as follows:

$$\begin{cases} f_s = \sigma_1 - \sigma_3 \frac{1 + \sin \varphi}{1 - \sin \varphi} + 2c \sqrt{\frac{1 + \sin \varphi}{1 - \sin \varphi}}, \\ f_t = \sigma_t - \sigma_3 \end{cases} \quad (1)$$

where  $\sigma_1$  is the maximum principal stress,  $\sigma_3$  is the minimum principal stress,  $c$  is the cohesion, and  $\varphi$  is the internal friction angle. From Equation 1, when  $f_s > 0$ , the coal-rock mass is damaged due to shear failure, and when  $f_s < 0$ , the coal-rock mass is damaged due to the tensile failure.

### 3 Numerical results

To study the distribution of the abutment pressure of the working face under different advancing steps, the monitoring points are arranged at three positions along the advancing direction of the working face, namely, the side of the transportation drift, the side of the return air drift, and the middle of the working face.

Based on the energy principle, the elastic strain energy density of coal-rock mass compiled by Fish language presented in FLAC<sup>3D</sup> is used to study the space–time distribution of elastic strain energy density in coal-rock mass in the stope under different advancing steps. The characteristics of strain energy are adopted to reveal the dynamic response in the mining process of the working face. By setting up coal pillars with different widths, the distribution of the inner abutment pressure and the residual elastic strain energy in the coal pillars under different coal pillar widths is obtained. The instability failure of the coal pillars in the isolated working face can be revealed. After the simulated calculation is completed, the values of the monitoring points are exported. The data processing software applications are used to obtain the distribution of the abutment pressure and elastic strain energy in front of the coal wall. The results are analyzed to obtain the cloud nephogram of the abutment pressure and the elastic strain energy in front of the coal wall. Finally, the stress distribution and the evolution of energy accumulation are quantitatively obtained.

### 3.1 Abutment pressure of the isolated working face

#### 3.1.1 Influence of the excavation step on abutment pressure

This section discusses the impact of different excavation steps on the hazard risk of an isolated working face by obtaining the distribution of abutment pressure in front of the isolated working face under seven excavation steps, namely, 30, 60, 90, 120, 150, 180, and 210 m. According to the built-in data output and post-processing functions, the stress of each unit of coal-rock strata is derived. Figure 4 shows the bearing abutment distribution in front of the coal wall of the isolated working face. It should be noted that the stress concentration coefficient is the ratio of the maximum stress to the average stress.

Figure 4 shows that the abutment pressure in front of the coal wall of the working face increases to the peak stress in a positive exponential relationship at first and then gradually decreases to the original rock stress in a negative exponential relationship, showing an upward convex trend. With the increase in the advancing step, the peak abutment pressure in front of the working face gradually increases, and the peak stress appears at 8–10 m in front of the working face. With the increase in the advancing step, the concentration coefficient of peak stress gradually increases, and the influence range of the abutment pressure of the working face gradually increases. When the working face advances 30 m, the peak abutment pressure in front of the coal wall of the working face is 36.7 MPa, and the stress concentration coefficient is 2.45. When the working face is advanced by 90 m, the peak abutment pressure in front of the working face is 49.5 MPa, and the stress concentration coefficient is 3.3. The hazard risk is relatively high when the working face is advanced by 30 m. When the advancing distance of the working face is advanced by 150 m, the peak abutment pressure in front of the working face is 58.5 MPa, and the stress concentration coefficient is 3.9. When the working face is advanced by 180 m, the peak abutment pressure in front of the working face is 63.3 MPa, and the stress concentration coefficient is 4.22. The stress concentration is relatively high when the working face is advanced by 90 m, and the hazard risk is correspondingly increased. When the advancing distance of the working face is advanced by 210 m, the peak abutment pressure in front of the coal wall is 69.8 MPa, and the stress concentration coefficient is 4.65. It can be further inferred

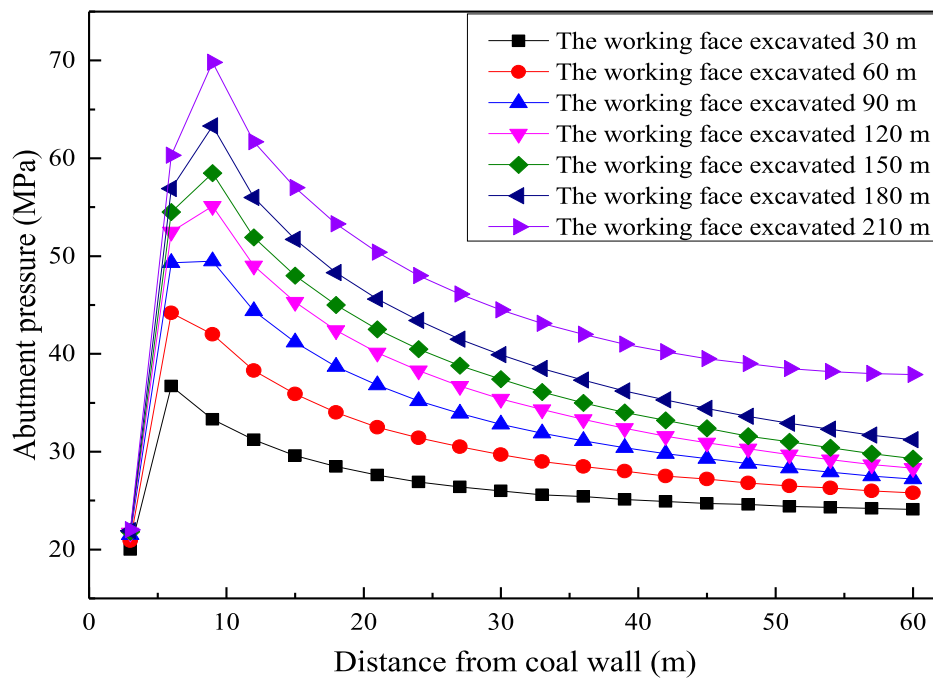


FIGURE 4  
Abutment pressure distribution of the working face in different advancing steps.

that with the continuous advancement of the working face, the stress gradient in front of the working face gradually increases. The stress concentration coefficient exceeds the critical value of the hazard risk, indicating that the hazard risk in the working face gradually increases.

### 3.1.2 Influence of buried depths on abutment pressure

In this section, we discuss the influence of different coal seam depths on the impact risk of isolated working faces by studying the distribution of the abutment pressure in front of the isolated working faces under three buried depths, namely, 400, 600, and 1,000 m.

The distribution of the abutment pressure in front of the island working face under different buried depths is shown in Figure 5. Figure 5 shows that the peak abutment pressure is 42 MPa when the buried depth of the coal seam is 400 m. The concentration coefficient is 4.2. The position of peak stress is 6 m away from the working face. When the buried depth of the coal seam is 600 m, the peak abutment pressure in front of the working face is 52.5 MPa. The concentration coefficient of peak stress is 3.5. The peak stress position is 8 m away from the coal wall of the working face. When the buried depth is 1,000 m, the peak abutment pressure in front of the working face is 84.6 MPa. The concentration coefficient of peak stress is 3.38. The position is 10 m away from the working face. Compared with the different buried depths of the coal seam, the peak abutment pressure in front of the coal wall gradually shifts to the deep part of the coal seam. With the increase in the buried depth, the abutment pressure in front of the coal wall increases first and then decreases. The underlying physical mechanisms of this phenomenon are multifaceted and involve the interaction of various factors. With the increase in the buried depth, the self-weight stress transmitted by

overlying strata is intensified, which causes the abutment pressure of working face to increase primarily. This phenomenon manifests itself in a more pronounced stress concentration as the coal-rock is subjected to enhanced compression. In addition, the mechanical properties of coal-rock change with the increase in buried depth. At deeper depths, the evolution of peak stress may migrate deeper into the coal seam, thus reducing the peak stress near the coal wall. In addition, as the depth of burial increases, the overlying rock tends to be rigid, thus storing more elastic energy, which leads to an increase in stress intensity. However, after a certain critical depth, the plasticity of coal-rock mass increases, the ability of rock strata to transfer stress weakens, and eventually, the peak stress decreases.

## 3.2 Elastic strain energy of the isolated working face

### 3.2.1 Elastic strain energy density

According to the principle of strain energy density of the elastomer under a three-dimensional stress state derived in elasticity,

$$U = \frac{1}{2} (\sigma_x \varepsilon_x + \sigma_y \varepsilon_y + \sigma_z \varepsilon_z + \tau_{yz} \gamma_{yz} + \tau_{zx} \gamma_{zx} + \tau_{xy} \gamma_{xy}), \quad (2)$$

where  $U$  is the strain energy density of the elastomer,  $\text{kJ}/\text{m}^3$ ;  $\sigma_x$ ,  $\sigma_y$ ,  $\sigma_z$ ,  $\tau_{yz}$ ,  $\tau_{zx}$ , and  $\tau_{xy}$  present six stress components at any point in the elastomer; and  $\varepsilon_x$ ,  $\varepsilon_y$ ,  $\varepsilon_z$ ,  $\gamma_{yz}$ ,  $\gamma_{zx}$ , and  $\gamma_{xy}$  present six strain components at any point in the elastomer.

The elastic body is regarded as an isotropic body. According to the generalized Hooke's law, the relationship between stress and

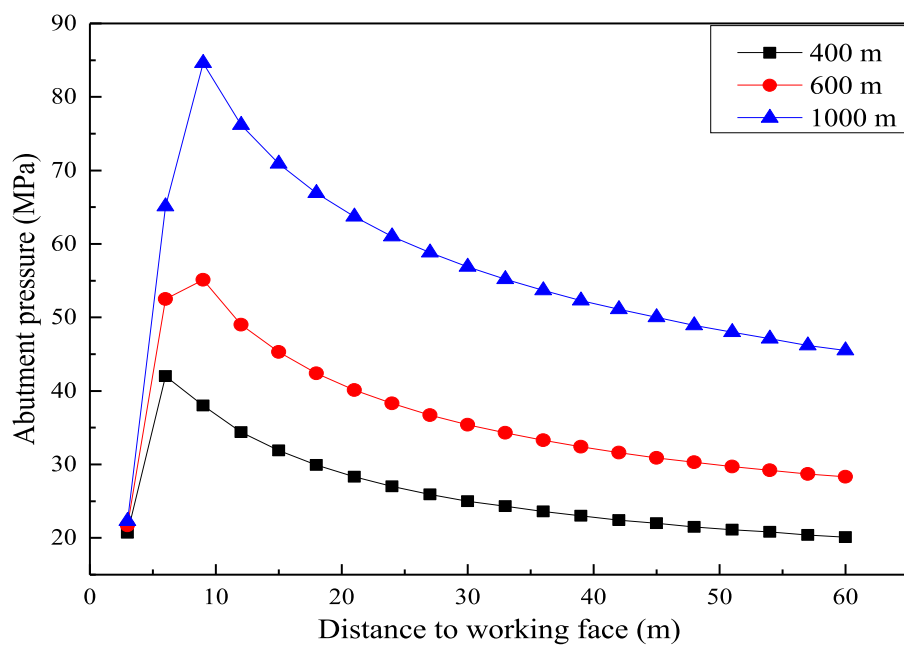


FIGURE 5  
Abutment pressure distribution of the front wall with various buried depths.

strain at any point in the elastic body is

$$\begin{cases} \varepsilon_x = \frac{1}{E} [\sigma_x - \mu(\sigma_y + \sigma_z)], \gamma_{yz} = \frac{1}{G} \tau_{yz} \\ \varepsilon_y = \frac{1}{E} [\sigma_y - \mu(\sigma_z + \sigma_x)], \gamma_{zx} = \frac{1}{G} \tau_{zx} \\ \varepsilon_z = \frac{1}{E} [\sigma_z - \mu(\sigma_x + \sigma_y)], \gamma_{xy} = \frac{1}{G} \tau_{xy} \end{cases} \quad (3)$$

where  $E$  is the modulus of elasticity,  $\mu$  is the lateral pressure coefficient, and  $G$  is the shear modulus.

There is a relationship among  $E$ ,  $\mu$ , and  $G$ :

$$G = \frac{E}{2(1+\mu)}. \quad (4)$$

Substituting Equations 3, 4 into Equation 2, the strain energy density expressed by the stress component is

$$U = \frac{(\sigma_x + \sigma_y + \sigma_z)^2 - 2(1+\mu)(\sigma_y\sigma_z + \sigma_z\sigma_x + \sigma_x\sigma_y - \tau_{yz}^2 - \tau_{zx}^2 - \tau_{xy}^2)}{2E}. \quad (5)$$

From Equation 5, it can be found that the strain energy of the roof rock under the three-dimensional stress state is in a quadratic relationship with its internal stress, that is, the higher the stress on the coal-rock in front of the coal wall, the greater the accumulated elastic strain energy.

### 3.2.2 Influence of the excavation step on elastic strain energy

Based on the built-in data output and post-processing functions of FLAC<sup>3D</sup>, six stress components of each unit of coal and rock strata in the middle of the working face are derived, and the elastic strain energy distribution of coal-rock strata along the advancing direction is calculated by substituting Equation 7, as shown in Figure 6.

Figure 6 shows that the peak strain energy gradually increases.

The peak elastic strain energy is located 8 m in front of the coal wall of the working face with increasing excavation steps. With the increase in the advancing distance of the working face, the elastic strain energy in front of the working face increases. The hazard risk in front of the working face increases accordingly. When the excavation step is 30 m, the peak strain energy is 136.43 kJ/m<sup>3</sup>. The roof rock layer of the working face is subject to large bending deformation, which causes elastic energy accumulation in the coal layer. Compared with the advancing distance of 30 m, the elastic strain energy in front of the coal wall of the working face increases slightly under the condition of the working face of 60 m. The peak strain energy density is 198.9 kJ/m<sup>3</sup>, and the peak strain energy also appears 8 m in front of the coal wall. When the working face is advanced by 90 m, the elastic strain energy in front of the working face continues to increase. The peak strain energy density is 248.27 kJ/m<sup>3</sup>. When the working face is advanced by 120 m, the peak elastic strain energy in front of the working face is 302.19 kJ/m<sup>3</sup>, which is significantly higher than that of 90 m. When the advancing distance of the working face is 150 m, the peak strain energy in front of the working face is 341.79 kJ/m<sup>3</sup>. When the excavation step is 180 m, the elastic strain energy density reaches 400.5 kJ/m<sup>3</sup>. When the working face is advanced by 210 m, the peak elastic strain energy reaches 485.65 kJ/m<sup>3</sup>.

In the process of underground coal mining, the forward movement of the working face will cause a change in the stress distribution in the front and adjacent areas of the coal seam, which has a significant impact on the coal pillar. These pillars absorb most of the stress transmitted by the overlying rock, resulting in a large expansion of the stress concentration area. This expansion is accompanied by a sharp increase in the elastic energy density within these regions. In addition, the advance of the working face disrupts

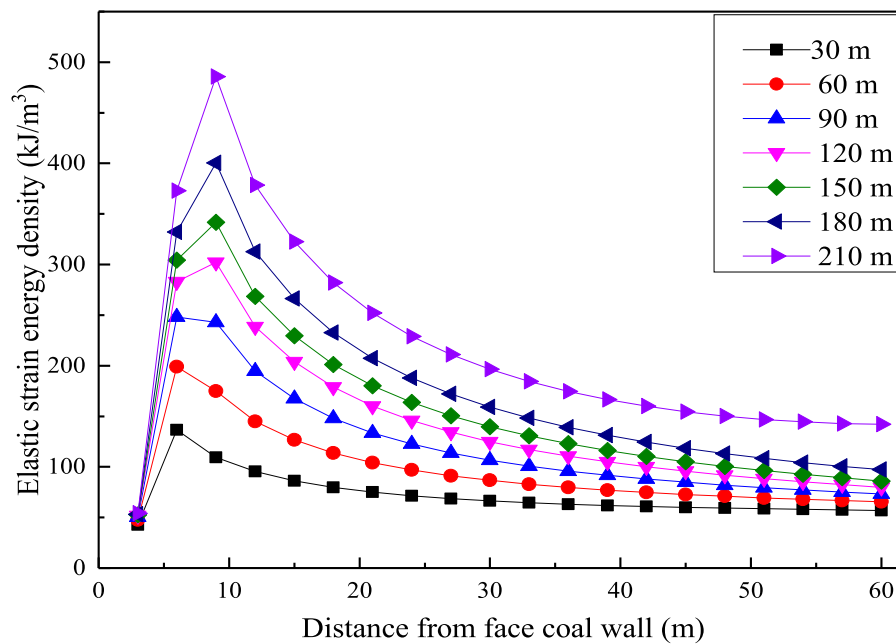


FIGURE 6  
Elastic strain energy distribution curve of the working face in the direction of face advance.

the initial stress balance, resulting in the elastic deformation of rock strata and coal seams. This deformation is physically manifested as an accumulation of energy or a significant increase in elastic energy density. With the increase in the mining step, the deformation of the coal seam and surrounding rock is more obvious, the stress adjustment speed is faster, and more elastic energy is accumulated. Therefore, with the advance of the working face and the increase in the mining step, the elastic energy density in the unexcavated coal seam in front also increases due to the continuous stress transfer process.

The relationship between the peak of strain energy density in front of the coal wall and the excavation step is fitted, as shown in Figure 7, and the fitting formula is obtained:

$$y = 0.44953 + 1.91453 * \exp(0.00396 * x). \quad (6)$$

From Equation 6, it can be found that the correlation coefficient  $R^2$  is 0.9704. With the increase in the excavation step, the peak elastic strain energy in front of the working face gradually increases, and the impact hazard of the working face also gradually increases.

### 3.2.3 Influence of burial depths on elastic strain energy

To reveal the influence of the burial depth on the strain energy of coal wall, this section takes a mining height of the coal seam of 7.5 m as the fixed value and the buried depth of the coal seam as the variable to investigate the evolution of elastic strain energy in front of the isolated working face under the three buried depths of 400, 600, and 1,000 m.

Based on the built-in data output and post-processing function of FLAC<sup>3D</sup>, the distribution curve of elastic strain energy density in front of the working face at different buried depths is calculated by

deriving six stress components of each unit of the coal rock strata under three cases of 400, 600, and 1,000 m, and substituting them into Equation 5, as shown in Figure 8. It can be found that the peak elastic strain energy in front of the working face is 181.07 kJ/m<sup>3</sup> when the mining depth is 400 m. The peak elastic strain energy density is 6 m away from the coal wall of the working face. When the buried depth is 600 m, the peak elastic strain energy in front of the working face is 302.19 kJ/m<sup>3</sup>. The distance between the peak strain energy is 9 m away from the coal wall of the working face. When the buried depth increases to 1,000 m, the peak elastic strain energy in front of the working face is 712.22 kJ/m<sup>3</sup>. The peak elastic strain energy is 10 m away from the coal wall of the working face. Compared with the burial depths of 400 and 600 m, the peak elastic strain energy gradually shifts to the inner of the coal seam when the burial depth increases to a deeper depth.

## 4 Coal burst risk assessment

### 4.1 Impact risk assessment of the 1,304 working face

The 1,304 working face is an island working face, and the mine has potential impact risk. To obtain the hazard score coordinates of the region, we can substitute the reaction values of the working face on different items and categories, which are (0, 1, 0), (0, 1, 0), (0, 0, 1), (1, 0, 0), (0, 1, 0), (0, 0, 1, 0), and (0, 0, 1) into the discriminant score function. Subsequently, the distance from this point to the center coordinates of the four grades are 0.3159, 0.3165, and 0.3155 m. Finally, according to the shortest distance theory, the score coordinate of the evaluation area is close to the center coordinate listed in Table 2 (level 4). Therefore, the impact hazard

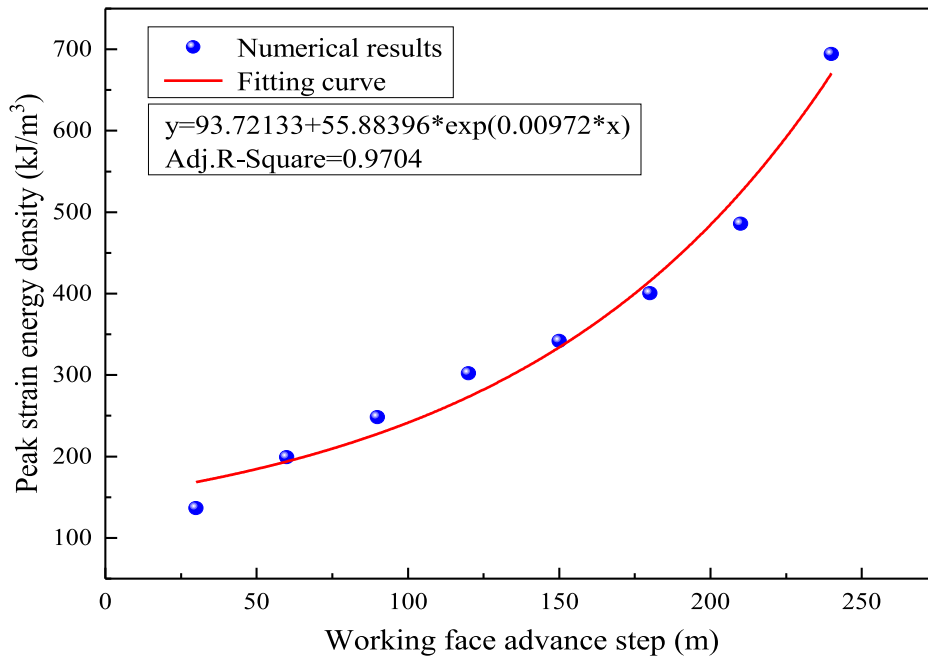


FIGURE 7 Fitting results of peak elastic strain energy density under different face advances.

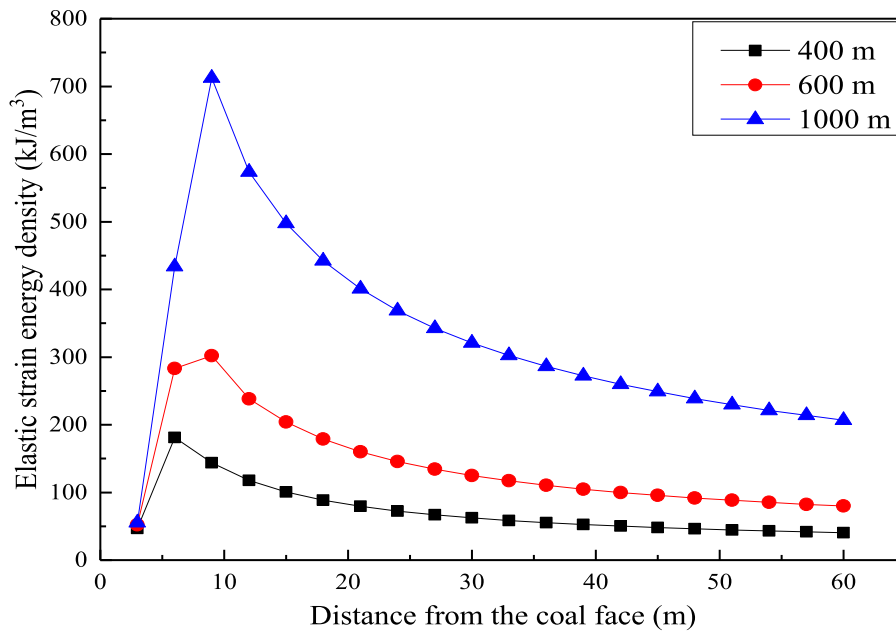


FIGURE 8 Elastic strain energy of the front wall under various mining depths.

level of the 1,304 island working face is 4; that is, it is a strong impact risk.

The coal burst of the working face is affected by numerous factors such as the physical and mechanical properties of coal-rock mass, geological overview, and mining technical conditions. In quantitative theory, qualitative variables are regarded as items. The

various possible situations of items are regarded as categories. Based on the analysis of the factors affecting the induced coal burst, the risk evaluation model of mine coal burst is established by using the relevant theory. The risk of mine regional coal burst is evaluated by using the evaluation model. Based on the specific mining conditions and geological situation of the working face, this study divides the

TABLE 2 Items and categories of the evaluation model.

Project	Category	Project	Category
X <sub>1</sub> : Coal seam impact tendency	C <sub>11</sub> : Weak impact C <sub>12</sub> : Medium impact C <sub>13</sub> : Strong impact	X <sub>5</sub> : Roof impact tendency	C <sub>51</sub> : Weak impact C <sub>52</sub> : Medium impact C <sub>53</sub> : Strong impact
X <sub>2</sub> : Dip angle of coal seam	C <sub>21</sub> : Near horizontal coal seam C <sub>22</sub> : Gently inclined coal seam C <sub>23</sub> : Inclined coal seam	X <sub>6</sub> : Horizontal tectonic stress	C <sub>61</sub> : High-level renovation C <sub>62</sub> : Medium-level renovation C <sub>63</sub> : Low-level reconstruction
X <sub>3</sub> : Coal seam thickness	C <sub>31</sub> : Medium thickness C <sub>32</sub> : Thick coal seam	X <sub>7</sub> : Degree of stress accumulation	C <sub>71</sub> : Low-level accumulation C <sub>72</sub> : Moderate-level accumulation C <sub>73</sub> : High-level accumulation
X <sub>4</sub> : Buried depth of the coal seam	C <sub>41</sub> : Less than 500 m C <sub>42</sub> : 500–700 m C <sub>43</sub> : Greater than 700 m		

coal burst risk degree of the island working face into four grades: 1, no coal burst risk; 2, weak shock hazard; 3, moderate shock hazard; and 4, strong shock hazard.

## 4.2 Quantitative theory modeling

In order to obtain modeling data, 60 modeling samples are determined from previous literature and engineering cases, that is, 16 level-1 samples ( $n_1 = 16$ ), 16 level-2 samples ( $n_2 = 16$ ), 16 level-3 samples ( $n_3 = 16$ ), and 12 level-4 samples ( $n_4 = 12$ ). It is specified that when a sample reacts on  $C_{jk}$  ( $j = 1, 2, 7; k = 1, 2, 3$ ), the value is 1; otherwise, it is 0. According to the major influencing factors inducing the impact hazard of the isolated working face, seven evaluation items are given. In the process of establishing the impact risk assessment model of the isolated working face, the key geomechanical and geotechnical conditions related to the impact risk of the isolated working face are studied by carefully analyzing the selected parameters. The bursting tendency of the coal seam is determined by examining the coal quality type, hardness, and explosive ability of the coal seam, which directly affect the response of the coal seam to sudden pressure change. There is a significant correlation between the hardness of coal and its bursting. The direction of the coal seam affects the stress distribution and may lead to increased stress concentration in some areas, thus increasing the risk of the isolated face. The thickness of the coal seam is the decisive factor of stress release in the process of extraction. The thicker the coal seam, the greater the elastic energy, the greater the energy released in the process of mining, and the greater the possibility of impact risk in the isolated working face. The buried depth affects the ground pressure of the coal seam, and the deeper coal seam bears more ground pressure, which increases the possibility and severity of stress concentration, and is easy to be harmed by the impact of the isolated working face. In addition, geological discontinuities, such as roof conditions, play a crucial role in explaining stress transfer within coal seams. The coal seam with a complex structure or through multiple fracture zones has greater risk of stress concentration and coal seam explosion. In addition, the site stress conditions and cumulative stress levels are

considered, which reflect the overall state of stress changes and stress accumulation caused by mining activities. Each project is divided into several categories, of which there are  $k$  categories in the  $j$  project. A total of 20 categories are listed in Table 2.

### 4.2.1 Modeling proposed

Using  $\delta_{ti}(j,k)$  represents the reaction value of the  $i$ th sample in the  $t$ th hazard level on the  $j$ th item and the  $k$ th category. After  $\delta_{ti}(j,k)$  is arranged in the original order, the reaction matrix is

$$X = (\delta_{ti}^t(j,k))_{60 \times 20}. \quad (7)$$

According to the quantitative theory, the risk score model is

$$y_i^t = \sum_{j=1}^7 \sum_{k=1}^{r_j} \delta_{ti}^t(j,k) b_{jk}, \quad (8)$$

where  $y_i^t$  is the risk score of the  $i$ th sample of the  $t$ th risk level and  $b_{jk}$  is the undetermined constant, which is called the category score and recorded as

$$y = (y_1^1, y_2^1, \dots, y_{16}^1, \dots, y_1^4, \dots, y_{12}^4)^T, \quad (9)$$

$$b = (b_{1,1}, b_{1,2}, \dots, b_{7,1}, b_{7,2}, b_{7,3})^T. \quad (10)$$

Then, Substituting Equations 9, 10 into Equation 8, can be expressed as

$$y = Xb. \quad (11)$$

According to the Fisher principle, the problem of category score  $b$  in Equation 11 can be transformed into finding the maximum characteristic root of its characteristic equation  $\lambda$ :

$$Cb = \lambda Db. \quad (12)$$

The corresponding equation satisfies the eigenvector:

$$b^T Db = 1. \quad (13)$$

Among Equations 12, 13,

$$C = \left( \bar{X} - \bar{\bar{X}} \right)^T \left( \bar{X} - \bar{\bar{X}} \right), \quad (14)$$

$$D = (X - \bar{X})^T (X - \bar{X}). \tag{15}$$

Equations 14, 15 are the inter-group dispersion matrix and total dispersion matrix, respectively. Among Equations 16–19, Both  $\bar{X} = \left( \begin{matrix} \bar{\delta}(j,k) \\ \vdots \end{matrix} \right)_{60 \times 20}$  and  $\bar{X} = \left( \begin{matrix} \bar{\delta}(j,k) \\ \vdots \end{matrix} \right)_{60 \times 20}$  have the same dimension as  $X$ .

$$\bar{X} = \begin{pmatrix} \bar{\delta}(1,1) \cdots \bar{\delta}(1,3) \bar{\delta}(2,1) \cdots \bar{\delta}(7,1) \cdots \bar{\delta}(7,3) \\ \bar{\delta}(1,1) \cdots \bar{\delta}(1,3) \bar{\delta}(2,1) \cdots \bar{\delta}(7,1) \cdots \bar{\delta}(7,3) \\ \dots \\ \bar{\delta}(1,1) \cdots \bar{\delta}(1,3) \bar{\delta}(2,1) \cdots \bar{\delta}(7,1) \cdots \bar{\delta}(7,3) \\ \bar{\delta}(1,1) \cdots \bar{\delta}(1,3) \bar{\delta}(2,1) \cdots \bar{\delta}(7,1) \cdots \bar{\delta}(7,3) \end{pmatrix}_{60 \times 20}, \tag{16}$$

$$\bar{\delta}(j,k) = \frac{1}{n} \sum_{i=1}^{n_i} \delta_i^t(j,k), \tag{17}$$

$$\bar{\delta}(j,k) = \frac{1}{60} \sum_{i=1}^4 \sum_{j=1}^{n_1} \delta_i^t(j,k) = \frac{1}{60} \sum_{i=1}^4 n_i \delta_i^t(j,k), \tag{18}$$

$$\bar{X} = \begin{pmatrix} \bar{\delta}^{(1)}(1,1) \cdots \bar{\delta}^{(1)}(1,3) \bar{\delta}^{(1)}(2,1) \cdots \bar{\delta}^{(1)}(7,1) \cdots \bar{\delta}^{(1)}(7,3) \\ \dots \\ \bar{\delta}^{(1)}(1,1) \cdots \bar{\delta}^{(1)}(1,3) \bar{\delta}^{(1)}(2,1) \cdots \bar{\delta}^{(1)}(7,1) \cdots \bar{\delta}^{(1)}(7,3) \\ \bar{\delta}^{(2)}(1,1) \cdots \bar{\delta}^{(2)}(1,3) \bar{\delta}^{(2)}(2,1) \cdots \bar{\delta}^{(2)}(7,1) \cdots \bar{\delta}^{(2)}(7,3) \\ \dots \\ \bar{\delta}^{(3)}(1,1) \cdots \bar{\delta}^{(3)}(1,3) \bar{\delta}^{(3)}(2,1) \cdots \bar{\delta}^{(3)}(7,1) \cdots \bar{\delta}^{(3)}(7,3) \\ \dots \\ \bar{\delta}^{(4)}(1,1) \cdots \bar{\delta}^{(4)}(1,3) \bar{\delta}^{(4)}(2,1) \cdots \bar{\delta}^{(4)}(7,1) \cdots \bar{\delta}^{(4)}(7,3) \\ \dots \\ \bar{\delta}^{(4)}(1,1) \cdots \bar{\delta}^{(4)}(1,3) \bar{\delta}^{(4)}(2,1) \cdots \bar{\delta}^{(4)}(7,1) \cdots \bar{\delta}^{(4)}(7,3) \end{pmatrix}_{60 \times 20} \tag{19}$$

As matrices  $C$  and  $D$  are singular matrices, we refer to the solution given by Dong (1979). The score vectors of three categories are calculated using MATLAB, and the corresponding characteristic roots are 1.10, 0.32, and 0.51, respectively.

$$y_1 = -0.03C_{12} - 0.05C_{13} + 0.04C_{22} + 0.03C_{23} + 0.01C_{32} - 0.02C_{42} - 0.06C_{43} - 0.05C_{52} + 0.07C_{53} - 0.01C_{62} + 0.22C_{63} + 0.11C_{72} + 0.26C_{73}, \tag{20}$$

$$y_1 = 0.13C_{12} - 0.05C_{13} - 0.13C_{22} - 0.08C_{23} - 0.22C_{32} + 0.03C_{42} - 0.21C_{43} - 0.19C_{52} - 0.01C_{53} + 0.05C_{62} + 0.06C_{63} - 0.23C_{72} - 0.07C_{73}, \tag{21}$$

$$y_1 = -0.05C_{12} - 0.06C_{13} + 0.17C_{22} - 0.03C_{23} + 0.01C_{32} - 0.12C_{42} - 0.20C_{43} - 0.13C_{52} + 0.06C_{53} - 0.01C_{62} + 0.06C_{63} - 0.05C_{72} - 0.17C_{73}. \tag{22}$$

The mean vector of the sample response of the  $t$ th risk level is recorded as

$$\left( \bar{\delta}^{(t)}(1,1), \dots, \bar{\delta}^{(t)}(1,3), \bar{\delta}^{(t)}(2,1), \dots, \bar{\delta}^{(t)}(7,1), \dots, \bar{\delta}^{(t)}(7,3) \right)^T. \tag{23}$$

The discriminant function is obtained by substituting it into Equations 20–23, and three scores are obtained, denoted as

TABLE 3 Center coordinates of different levels.

Level	Central coordinates
1	(−0.04, −0.27, −0.18)
2	(0.00, −0.40, −0.03)
3	(0.11, −0.41, −0.27)
4	(0.24, −0.27, −0.13)

TABLE 4 Hazard risk evaluation of the 1,304 island working face.

Level		Error magnitude		
		One-dimensional	Two-dimensional	Three-dimensional
1	16	2	1	2
2	16	1	2	1
3	16	2	2	1
4	12	2	1	1
Accuracy		88%	90%	91.7%

$y_1^{(t)}, y_2^{(t)}, y_3^{(t)}$  and recorded as

$$V^{(t)} = (y_1^{(t)}, y_2^{(t)}, y_3^{(t)})^T. \tag{24}$$

$V(t)$  is the central coordinate of the sample score of the  $t$ th hazard level, and the central coordinates of the four levels are obtained from Equation 24, as listed in Table 3.

The evaluation standard is based on the principle of minimum distance. Taking 3D analysis as an example, a certain place in the mine is considered, its response value  $\delta(j,k)$  on various items is investigated and brought into the discriminant function, and three scores, namely,  $y_1, y_2,$  and  $y_3,$  are obtained, recorded as  $V = (y_1, y_2, y_3)^T$ . In  $l$  dimensional Euclidean space, the distance from inspection point  $v$  to each central coordinate  $X$ . If  $\|V - V^{(t_0)}\| = \min_t \|V - V^{(t)}\|$ , then the impact grade here is  $\|V - V^{(t_0)}\| = \min \|V - V^{(t)}\|$ .

### 4.2.2 Modeling verification

The model has three scoring functions, so one-dimensional, two-dimensional, and three-dimensional evaluation methods can be used to train the model. The test results of the one-dimensional evaluation analysis are only the first score function and the first component of  $(V_1 - V_4)$ ; the two-dimensional evaluation analysis using the first two score functions and the first two components of  $(V_1 - V_4)$  and the three-dimensional evaluation analysis are listed in Table 4.

Table 4 shows that compared with the 1D and 2D evaluation results, the accuracy obtained using the 3D analysis method is higher, and the corresponding evaluation effect is relatively ideal. Therefore, the 1D and 2D analysis results are ignored. Finally, the 3D evaluation results are taken as the analysis method of hazard risk evaluation of 1,304 island working face in this study.

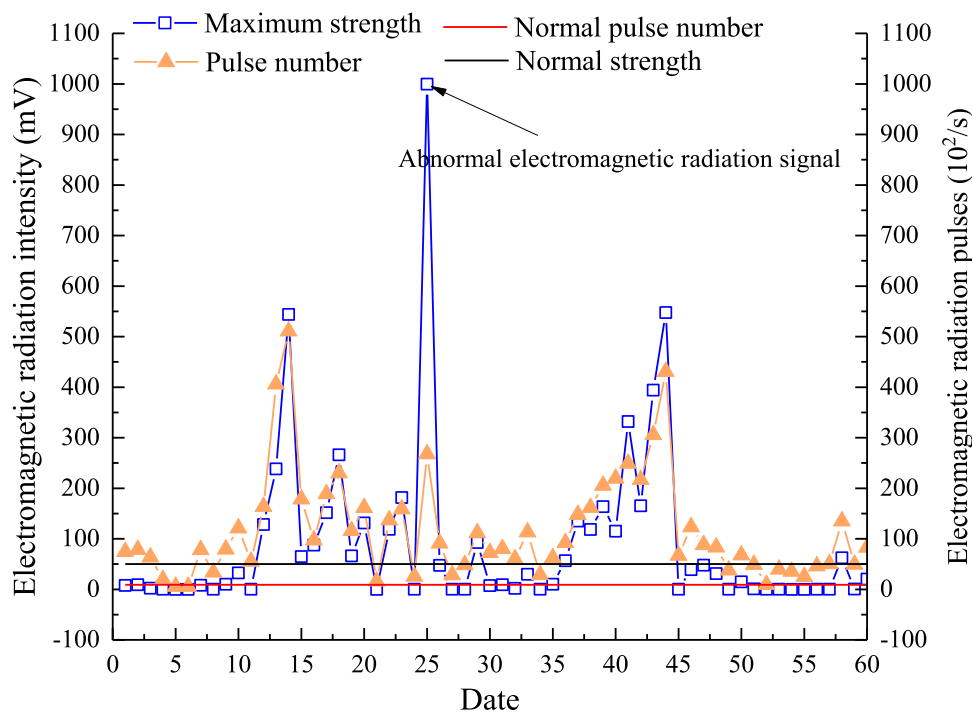


FIGURE 9 Evolution of the electromagnetic radiation signal at an advance of 30 m of the working face (Wang et al., 2014).

### 4.3 Analysis of electromagnetic radiation of 1,304 working face

It is well known that electromagnetic radiation from coal-rock is a phenomenon where electromagnetic energy is emitted outward during the deformation and fracture of coal-rock under load. The occurrence of a rock burst is the process of mass energy release when the strength limit of the coal-rock mass is reached after the process of energy accumulation. Figure 9 shows the evolution of electromagnetic radiation information in the advanced roadway in front of the coal wall of the working face. It is important to note that the horizontal axis dates in Figure 9 range from 1 August 2012 to 30 September 2012. As observed in Figure 9, the electromagnetic radiation intensity and pulse number of the coal body fluctuated around the normal value during August 1–August 8 and August 27–September 4, indicating that the internal stress level of the coal body was normal during these two periods. From August 9 to August 14 and from September 5 to September 12, the electromagnetic radiation intensity and pulse number of coal continued to increase significantly, with the amplitude of increase reaching or even exceeding about 10 times the normal value, suggesting a sharp increase in stress during these periods. The higher stress levels led to intensified internal fracturing and friction within coal, resulting in stronger electromagnetic radiation signals. On August 25, an abnormal electromagnetic radiation signal with a pulse number of up to  $1 \times 10^5$  was recorded, which was analyzed as an electromagnetic field interference signal. Before the “8.14 event” and “9.12 event,” the electromagnetic radiation

intensity and pulse number of the coal body had been continuously increasing. It can be concluded that there is usually a period of continuous increase in the internal stress of the coal body before a rock burst occurs, and it is the continuous and sharp increase in the internal stress of the coal body that triggers the rock burst event.

Based on the above analysis, it was found that the silent period of micro-seismic events, the continuously increasing period of electromagnetic radiation intensity of the coal body, and the continuously increasing period of the electromagnetic radiation pulse number of the coal body are the precursor information of rock burst. These precursor information are converted into early-warning parameters of rock burst, and a multi-parameter early-warning method of rock burst precursor information needs to be proposed. Therefore, when the working face is judged to be at risk of rock burst, the drilling cutting method is used to identify the localized areas at risk of rock burst. Subsequently, pressure relief measures such as blasting, coal seam water injection, and drilling pressure-relieving holes are used to decompress and mitigate the risk in the coal seam until the danger of rock burst is eliminated.

## 5 Conclusion

- (1) With the increase in the advancing step, the abutment pressure and elastic strain energy density in front of the working face increase to the maximum in a positive exponential relationship at first and then decrease due to *in situ* stress, which presents

an upward convex trend. The influence range of the abutment pressure of the working face gradually increases.

- (2) With the increase in coal thickness and burial depth, the peak abutment pressure and elastic strain energy density in front of the coal wall gradually increase. The position of occurrence gradually moves away from the coal wall. The concentration coefficient of peak strength gradually increases, indicating that the deeper the coal seam is, the greater the possibility of coal burst.
- (3) Based on the quantitative theory and the minimum distance principle, the impact risk assessment model of isolated working faces is established. Compared with the evaluation results of one-dimensional and two-dimensional analyses, the accuracy of the three-dimensional analysis method is relatively higher, indicating that the accuracy of the evaluation effect is higher.

## Data availability statement

The original contributions presented in the study are included in the article/Supplementary Material; further inquiries can be directed to the corresponding author.

## Author contributions

GL: methodology and writing—original draft. RL: funding acquisition and writing—review and editing. LH: software, visualization, and writing—original draft. ML: data curation, formal analysis, and writing—original draft. JZ: data curation, formal analysis, and writing—original draft.

## References

- Ahmad, M., Hu, J. L., Hadzima-Nyarko, M., Ahmad, F., Tang, X. W., Rahman, Z. U., et al. (2021). Rock burst hazard prediction in underground projects using two intelligent classification techniques: a comparative study. *Symmetry* 13 (4), 632. doi:10.3390/sym13040632
- Cao, A. Y., Liu, Y. Q., Yang, X., Li, S., and Liu, Y. P. (2022). FDNNet: knowledge and data fusion-driven deep neural network for coal burst prediction. *Sensors (Basel)* 22 (8), 3088. doi:10.3390/s22083088
- Cao, J. R., Dou, L. M., He, J., Xie, J. H., Han, Z. P., and Wang, S. W. (2023). Mechanism of the coal bursts in the working face during mining of steeply inclined and extra thick coal seam. *Geomatics, Nat. Hazards Risk* 14 (1), 2206511. doi:10.1080/19475705.2023.2206511
- Di, Y. Y., Wang, E. Y., Li, Z. H., Liu, X. F., Huang, T., and Yao, J. J. (2023). Comprehensive early warning method of microseismic, acoustic emission, and electromagnetic radiation signals of rock burst based on deep learning. *Int. J. Rock Mech. Min. Sci.* 170, 105519. doi:10.1016/j.ijrmms.2023.105519
- Dong, H. S., Zhao, K. Y., and Li, M. (2013). Improvement of analytic hierarchy process and its application for coal mine safety assessment. *Appl. Mech. Mater.* 368–370, 1979–1984. doi:10.4028/www.scientific.net/amm.368-370.1979
- Dong, W. Q., Zhou, G. Y., and Xia, X. (1979). The theory of quantification and its application [M]. Changchun: Jilin People Publishing House.
- Dou, L. M., Cai, W., Cao, A. Y., and Guo, W. C. (2018). Comprehensive early warning of rock burst utilizing microseismic multi-parameter indices. *Int. J. Environ. Sci. Tech.* 28, 767–774. doi:10.1016/j.ijmst.2018.08.007
- Du, J. S., Chen, J., Pu, Y. Y., Jiang, D. Y., Chen, L. L., and Zhang, Y. R. (2021). Risk assessment of dynamic disasters in deep coal mines based on multi-source, multi-parameter indexes, and engineering application. *Process Saf. Environ. Prof.* 155, 575–586. doi:10.1016/j.psep.2021.09.034
- Guo, W. Y., Gu, Q. H., Tan, Y. L., and Hu, S. C. (2019). Case studies of rock bursts in tectonic areas with facies change. *Energies* 12 (7), 1330. doi:10.3390/en12071330
- Guo, W. Y., Zhao, T. B., Tan, Y. L., Yu, F. H., Hu, S. C., and Yang, F. Q. (2017). Progressive mitigation method of rock bursts under complicated geological conditions. *Int. J. Rock Mech. Min. Sci.* 96, 11–22. doi:10.1016/j.ijrmms.2017.04.011
- Hao, X. T., and Niu, H. (2014). Research on gas content prediction model of hebi No. 6 mine based on quantification theory. *Appl. Mech. Mater.* 3044 (535), 614–621. doi:10.4028/www.scientific.net/amm.535.614
- He, J., Dou, L. M., Gong, S. Y., Li, J., and Ma, Z. Q. (2017). Rock burst assessment and prediction by dynamic and static stress analysis based on microseismic monitoring. *Int. J. Rock Mech. Min. Sci.* 93, 46–53. doi:10.1016/j.ijrmms.2017.01.005
- He, M. C., Cheng, T., Qiao, Y. F., and Li, H. R. (2023). A review of rockburst: experiments, theories, and simulations. *J. Rock Mech. Geotech. Eng.* 15 (5), 1312–1353. doi:10.1016/j.jrmge.2022.07.014
- Hu, X. C., Yang, S. Q., Zhou, X. H., Zhang, G. X., and Xie, B. B. (2014). A quantification prediction model of coalbed methane content and its application in Pannan coalfield, Southwest China. *J. Nat. Gas. Sci. Eng.* 21, 900–906. doi:10.1016/j.jngse.2014.10.017
- Li, P., Liu, Y., Cai, M. F., Miao, S. J., Dai, L. P., and Gorjian, M. (2024). Accurate stress measurement using hydraulic fracturing in deep low-permeability reservoirs: challenges and research directions. *Adv. Geo-Energy Res.* 14 (3), 165–196. doi:10.46690/ager.2024.12.02
- Li, S. J., Kuang, Z. H., Xiao, Y. X., Qiao, Z. B., and Yang, W. B. (2022). Rockburst tendency prediction based on an integrating method of combination weighting and matter-element extension theory: a case study in the Bayu Tunnel of the Sichuan-Tibet railway. *Eng. Geol.* 308, 106796. doi:10.1016/j.enggeo.2022.106796
- Li, X. L., Chen, S. J., Wang, E. Y., and Li, Z. H. (2021). Rockburst mechanism in coal rock with structural surface and the microseismic (MS) and electromagnetic radiation (EMR) response. *Eng. Fail. Anal.* 124, 105396. doi:10.1016/j.engfailanal.2021.105396

## Funding

The author(s) declare that financial support was received for the research, authorship, and/or publication of this article. This study was financially supported by the China Postdoctoral Science Foundation (No. 2023MD744136), the Special Project of Postdoctoral Research in Chongqing (No. 2022CQBSHTB3109), the Opening Project of the Key Laboratory of Safety and High-efficiency Coal Mining, Ministry of Education (JYBSYS202306), and the Opening Project of Sichuan Province University Key Laboratory of Bridge Non-destruction Detecting and Engineering Computing (2022QZJ01), Aid Program for the Science and Technology Innovative Research Team in Higher Educational Institutions of Hunan Province.

## Conflict of interest

The authors declare that the research was conducted in the absence of any commercial or financial relationships that could be construed as a potential conflict of interest.

## Publisher's note

All claims expressed in this article are solely those of the authors and do not necessarily represent those of their affiliated organizations, or those of the publisher, the editors, and the reviewers. Any product that may be evaluated in this article, or claim that may be made by its manufacturer, is not guaranteed or endorsed by the publisher.

- Liu, Y., Ouyang, Z. H., Yi, H. Y., and Qin, H. Y. (2023). Study of the multilevel fuzzy comprehensive evaluation of rock burst risk. *Sustainability* 15 (17), 13176. doi:10.3390/su151713176
- Pan, J., Liu, S., Qin, Z., Wang, S., Zhang, C., and Ma, W. (2018). Mechanism and prevention of concentrated static load type rock burst of roadway group in deep mining area. *J. China Coal Soc.* 43 (10), 2679–2686. doi:10.13225/j.cnki.jccs.2018.0016
- Sun, J., Wang, L. G., Zhang, H. L., Wang, L. G., and Shen, Y. F. (2009). Application of fuzzy neural network in predicting the risk of rock burst. *Procedia Earth Planet. Sci.* 1 (1), 536–543. doi:10.1016/j.proeps.2009.09.085
- Tai, Y., Yu, B., Kuang, T. J., Shi, B. W., Meng, X. B., and Fu, M. Q. (2022). An innovative technology of fracturing hard strata from the ground for precontrol of rock burst in a coal mine. *Energy Sci. Eng.* 11, 565–584. doi:10.1002/ese3.1346
- Tang, S. F., Tong, M. M., Qin, H. P., Hu, J. L., and He, X. M. (2010). The acoustic emission experiment system of rock outburst in water inrush. *J. Min. Saf. Eng.* 27 (03), 429–432 + 437.
- Wang, C. L., Wu, A. X., Lu, H., Bao, T. C., and Liu, X. H. (2015). Predicting rock burst tendency based on fuzzy matter-element model. *Int. J. Rock Mech. Min. Sci.* 75, 224–232. doi:10.1016/j.ijrmms.2015.02.004
- Wang, C. Q., Jiang, B. Y., Gu, S. T., Tan, Y. L., Wang, R. C., and Huang, R. F. (2014). Study of precursor information recognition and multiparameter early warning before rockburst of island fully mechanized caving face. *Rock Soil Mech.* 35 (12), 3523–3530. doi:10.16285/j.rsm.2014.12.023
- Wang, J. X., Wang, E. Y., Yang, W. X., Li, B. L., Li, Z. H., and Liu, X. F. (2022). Rock burst monitoring and early warning under uncertainty based on multi-information fusion approach. *Measurement* 205, 112188. doi:10.1016/j.measurement.2022.112188
- Wang, P., Gu, S. C., and Sun, W. (2024). Roadway rock burst prediction based on catastrophe theory. *Sci. Rep.* 14, 7321. doi:10.1038/s41598-024-58072-0
- Wang, X., Liu, S., Liu, X., Shan, T., Zhou, X., Xie, H., et al. (2024b). Mode I fracture propagation and post-peak behavior of sandstone: insight from AE and DIC observation. *Eng. Fract. Mech.* 302 (110093), 110093–110115. doi:10.1016/j.engfracmech.2024.110093
- Wang, X., Liu, X., Wang, E., Liu, S., Shan, T., and Labuz, J. F. (2024a). Microcracking characterization in tensile failure of hard coal: an experimental and numerical approach. *Rock Mech. Rock Eng.* 57, 6441–6460. doi:10.1007/s00603-024-03827-4
- Wang, X. Z., Chen, J. J., Li, P., She, X., and Niu, G. Y. (2012). Gas leakage prediction model of large-scale explosions in hard rock based on quantification theory. *Transp. Porous Med.* 95 (1), 171–183. doi:10.1007/s11242-012-0037-6
- Wen, J. L., Li, H. S., Jiang, F. X., Yu, Z. X., Ma, H. T., and Yang, X. L. (2019). Rock burst risk evaluation based on equivalent surrounding rock strength. *Int. J. Min. Sci. Technol.* 29 (4), 571–576. doi:10.1016/j.ijmst.2019.06.005
- Wu, S. C., Wu, Z. G., and Zhang, C. X. (2019). Rock burst prediction probability model based on case analysis. *Tunn. Undergr. Sp. Tech.* 93, 103069. doi:10.1016/j.tust.2019.103069
- Wu, Z. J., and Wong, L. N. Y. (2012). Frictional crack initiation and propagation analysis using the numerical manifold method. *Comput. Geotech.* 39, 38–53. doi:10.1016/j.compgeo.2011.08.011
- Xie, H. P., Gao, F., Ju, Y., Gao, M. Z., and Xie, L. Z. (2015). Quantitative definition and investigation of deep mining. *J. China Coal Soc.* 40 (01), 1–10. doi:10.13225/j.cnki.jccs.2014.1690
- Xu, L. M., Lu, K. X., Pan, Y. S., and Qin, Z. J. (2019). Study on rock burst characteristics of coal mine roadway in China. *Energy Sources, Part A Recovery, Util. Environ. Eff.* 44 (2), 3016–3035. doi:10.1080/15567036.2019.1655114
- Zhao, T. B., Guo, W. Y., Tan, Y. L., Lu, C. P., and Wang, C. W. (2018b). Case histories of rock bursts under complicated geological conditions. *B. Eng. Geol. Environ.* 77, 1529–1545. doi:10.1007/s10064-017-1014-7
- Zhao, T. B., Guo, W. Y., Tan, Y. L., Yin, Y. C., Cai, L. S., and Pan, J. F. (2018a). Case studies of rock bursts under complicated geological conditions during multi-seam mining at a depth of 800 m. *Rock Mech. Rock Eng.* 51, 1539–1564. doi:10.1007/s00603-018-1411-7
- Zhou, J., Chen, C., Wei, C., and Du, K. (2022). An improved connection cloud model of an updated database: a multicriteria uncertainty model for coal burst liability evaluation. *Nat. Resour. Res.* 31, 1687–1704. doi:10.1007/s11053-022-10042-x
- Zhou, K. Y., Dou, L. M., Li, X. W., Song, S. K., Cao, J. R., Bai, J. Z., et al. (2022). Coal burst and mining-induced stress evolution in a deep isolated main entry area-A case study. *Eng. Fail. Anal.* 137, 106289. doi:10.1016/j.engfailanal.2022.106289